

A 2-D Hypersingular Time-Domain BEM for Dynamic Crack Analysis in Generally Anisotropic Solids

S. Beyer¹, Ch. Zhang², S. Hirose³, J. Sladek and V. Sladek⁴

Abstract: This paper presents a hypersingular time-domain boundary element method (BEM) for transient dynamic crack analysis in two-dimensional (2-D), homogeneous, anisotropic and linear elastic solids. A finite crack in an infinite or a finite solid subjected to impact loading conditions is investigated. A combination of the classical displacement boundary integral equations (BIEs) on the external boundary and the hypersingular traction BIEs on the crack-faces is applied. The present BEM uses the time-domain dynamic fundamental solutions for anisotropic solids derived by Wang and Achenbach (1994). An explicit time-stepping scheme based on collocation method is developed. Numerical examples for computing the dynamic stress intensity factors (SIFs) are presented and discussed.

Keyword: Hypersingular time-domain BEM, Collocation method, Transient elastodynamic crack analysis, Anisotropic elastic solids

1 Introduction

Dynamic crack analysis is of special importance to linear elastic fracture mechanics and quantitative non-destructive material testing by ultrasonics or acoustic emission. Time-domain boundary integral equation method (BIEM) or boundary element method (BEM) provides an efficient and accurate numerical tool for this purpose. Although the BIEM/BEM has been suc-

cessfully applied to dynamic analysis of homogeneous, isotropic and linear elastic solids since many years (e.g., Aliabadi, 2002; Antes, 1985, 1987; Beskos, 1987, 1997; Bonnet, 1999; Cruse and Rizzo, 1968; Cruse, 1968; Cole et al., 1978; Dominguez, 1993; Estorff, 1986; Manolis, 1983; Mansur, 1983; Niwa et al., 1980), its applications to anisotropic and linear elastic solids are yet still very limited. The main reason lies in the fact that in contrast to homogeneous, isotropic and linear elastic solids, the fundamental solutions for homogeneous, anisotropic and linear elastic solids cannot be given in an explicit form and they have a much more complicated mathematical structure, which may affect the numerical implementation and the efficiency of the time-domain BEM for transient dynamic crack analysis in generally anisotropic solids. Recent developments on time-domain BIEM/BEM for homogeneous, anisotropic and linear elastic solids with holes or cracks have been reported by Wang, Achenbach and Hirose (1996), Hirose (1999), Hirose, Wang and Achenbach (2000), Zhang (2000, 2002a,b), Zhang, Savaidis and Savaidis (2001), Hirose, Zhang and Wang (2002), Tan, Hirose, Zhang and Wang (2005), Tan, Hirose and Zhang (2005). A review on dynamic crack analysis in anisotropic solids has been given by Zhang (2004).

In this paper, a 2-D hypersingular time-domain BEM is presented for transient dynamic crack analysis in infinite and finite anisotropic solids with a finite crack under impact loading conditions. A combination of the classical displacement boundary integral equations (BIEs) on the external boundary and the hypersingular traction BIEs on the crack-faces is used. The method applies the time-domain elastodynamic fundamental solutions for anisotropic solids, which have

¹ Department of Civil Engineering, University of Applied Sciences Zittau/Görlitz, D-02763 Zittau, Germany

² Chair of Structural Mechanics, Department of Civil Engineering, University of Siegen, D-57068 Siegen, Germany

³ Department of Mechanical and Environmental Informatics, Tokyo Institute of Technology, Tokyo 152-8552, Japan

⁴ Institute of Construction and Architecture, Slovak Academy of Sciences, 84503 Bratislava, Slovakia

been derived by Wang and Achenbach (1994). In 2-D case, the time-domain elastodynamic fundamental solutions for anisotropic solids can be decomposed into a time-independent singular static part and a regular dynamic part, which can be expressed in terms of line integrals over a unit-circle. To solve the strongly singular and hyper-singular time-domain BIEs numerically, an explicit time-stepping scheme is developed. For both spatial and temporal discretizations a collocation method is adopted. A linear temporal shape-function is applied for the temporal approximation of the boundary data. For the spatial approximation of the boundary data, two different kinds of spatial shape-functions are implemented. A “square-root” crack-tip shape-function is chosen for boundary elements adjacent to the crack-tips, while for all other boundary elements a constant spatial shape-function is used. Time integrations of the system matrices are performed analytically, while strongly singular and hyper-singular spatial boundary integrals are treated by special analytical and numerical techniques. To verify the accuracy of the present time-domain BEM, several numerical examples for the dynamic stress intensity factors (SIFs), which can be directly obtained from the numerically computed crack-opening-displacements (CODs), are presented and discussed.

2 Problem formulation and time-domain BIEs

Let us consider a homogeneous, anisotropic and linear elastic solid containing a crack in a 2-D plane as depicted in Fig. 1. Here, Γ_{ex} denotes the external boundary of the linear elastic solid and Γ_c^+ and Γ_c^- represent the upper and the lower crack-face of the crack. In the absence of body forces, the cracked solid satisfies the equations of motion and Hooke's law

$$\sigma_{ij,j} = \rho \ddot{u}_i, \quad (1)$$

$$\sigma_{ij} = C_{ijkl} u_{k,l}, \quad (2)$$

where σ_{ij} and u_i represent the stress and the displacement components, ρ is the mass density, and C_{ijkl} is the 4th-order elasticity tensor. Throughout the analysis, superscript dots denote deriva-

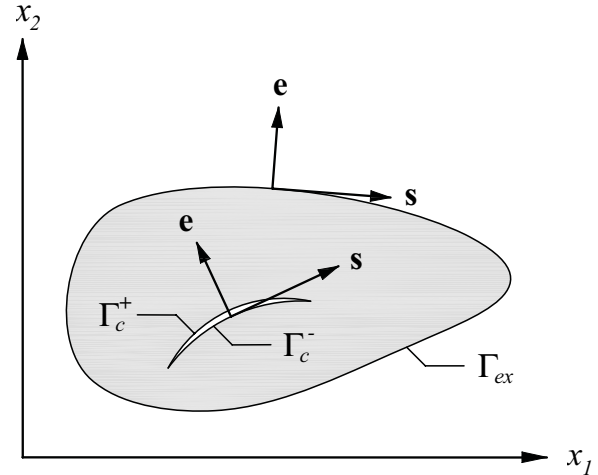


Figure 1: A crack in an anisotropic solid

tives with respect to time, and a comma after a quantity represents spatial derivatives.

In the present boundary integral equation formulation, a combination of the classical displacement BIEs and the traction BIEs is used. The classical displacement BIEs are applied to the external boundary Γ_{ex} of the cracked solid, which can be written as

$$\begin{aligned} \delta(\mathbf{x})u_k(\mathbf{x},t) = & \int_{\Gamma_{ex}} [g_{ik}(\mathbf{x},\mathbf{y};t) * f_i(\mathbf{y},t) - h_{ik}(\mathbf{x},\mathbf{y};t) * u_i(\mathbf{y},t)] ds_y \\ & + \int_{\Gamma_c} h_{ik}(\mathbf{x},\mathbf{y};t) * \Delta u_i(\mathbf{y},t) ds_y, \quad \mathbf{x} \in \Gamma_{ex} \quad (3) \end{aligned}$$

where f_i are the traction components, Δu_i denotes the CODs, Γ_c represents the lower crack-face, and $\delta(\mathbf{x})$ is a constant term depending on the smoothness of the boundary. Also, an asterisk in Eq. (3) denotes the Riemann convolution, which is defined by

$$g_{ik}(\mathbf{x},\mathbf{y};t) * f_i(\mathbf{y},t) = \int_0^t g_{ik}(\mathbf{x},\mathbf{y};t-\tau) f_i(\mathbf{y},\tau) d\tau. \quad (4)$$

Furthermore, g_{ik} and h_{ik} in Eq. (3) are the time-domain elastodynamic fundamental solutions for homogeneous, anisotropic and linear

elastic solids, which have been derived by Wang and Achenbach (1994) via Radon transform. They can be expressed as line integrals over a unit circle

$$g_{ik}(\mathbf{x}, \mathbf{y}; t) = \frac{H(t)}{4\pi^2} \int_{|n|=1} \sum_{l=1}^L \frac{P_{ik}^l}{\rho c_l c_l t + \mathbf{n} \cdot (\mathbf{y} - \mathbf{x})} d\mathbf{n}, \quad (5)$$

$$\begin{aligned} h_{ik}(\mathbf{x}, \mathbf{y}; t) &= C_{i\gamma p \delta} e_\gamma(\mathbf{y}) \frac{\partial g_{pk}(\mathbf{x}, \mathbf{y}; t)}{\partial y_\delta} \\ &= \frac{H(t)}{4\pi^2} \frac{\partial}{\partial t} \int_{|n|=1} \sum_{l=1}^L \frac{Q_{ik}^l[\mathbf{n}, \mathbf{e}(\mathbf{y})]}{\rho c_l^2} \frac{d\mathbf{n}}{c_l t + \mathbf{n} \cdot (\mathbf{y} - \mathbf{x})}, \end{aligned} \quad (6)$$

where $H(t)$ denotes the Heaviside function, c_l are the phase wave velocities, and $e_\gamma(\mathbf{y})$ denote the components of the outward unit normal vector at \mathbf{y} . Also, P_{ik}^l and ρc_l^2 represent the projection operator and the eigenvalues of the Christoffel matrix

$$\Gamma_{ik}(n_1, n_2) = C_{i\alpha k \beta} n_\alpha n_\beta. \quad (7)$$

The projection operator P_{ik}^l in Eq. (5) is defined by

$$P_{ik}^l = \frac{E_{ik}^l}{E_{qq}^l}, \quad (8)$$

in which

$$E_{ik}^l = E_{ik}(c_l, n_1, n_2) = \text{adj} [\Gamma_{ik}(n_1, n_2) - \rho c_l^2 \delta_{ik}], \quad (9)$$

and δ_{ik} is the Kronecker delta. In Eq. (6), Q_{ik}^l is determined by

$$Q_{ik}^l(\mathbf{n}, \mathbf{e}) = C_{i\gamma p \delta} e_\gamma(\mathbf{y}) n_\delta P_{pk}^l(\mathbf{n}). \quad (10)$$

The following traction boundary integral equations are used on the crack-face Γ_c

$$\begin{aligned} \delta(\mathbf{x}) f_j(\mathbf{x}, t) &= \\ &\int_{\Gamma_{\text{ex}}} [\hat{h}_{ij}(\mathbf{x}, \mathbf{y}; t) * f_i(\mathbf{y}, t) - w_{ij}(\mathbf{x}, \mathbf{y}; t) * u_i(\mathbf{y}, t)] ds_y \\ &+ \int_{\Gamma_c} w_{ij}(\mathbf{x}, \mathbf{y}; t) * \Delta u_i(\mathbf{y}, t) ds_y, \quad \mathbf{x} \in \Gamma_c, \end{aligned} \quad (11)$$

with w_{ij} being the higher-order elastodynamic traction fundamental solution defined by

$$\begin{aligned} w_{ij}(x, y; t) &= C_{j\alpha k \beta} e_\alpha(\mathbf{x}) C_{i\gamma p \delta} e_\gamma(\mathbf{y}) \frac{\partial}{\partial x_\beta} \frac{\partial}{\partial y_\delta} g_{pk}(\mathbf{x}, \mathbf{y}; t) \\ &= -\frac{H(t)}{4\pi^2} \times \\ &\frac{\partial^2}{\partial t^2} \int_{|n|=1} \sum_{l=1}^L \frac{R_{ij}^l[\mathbf{n}, \mathbf{e}(\mathbf{x}), \mathbf{e}(\mathbf{y})]}{\rho c_l^3} \frac{d\mathbf{n}}{c_l t + \mathbf{n} \cdot (\mathbf{y} - \mathbf{x})}, \end{aligned} \quad (12)$$

where

$$\begin{aligned} R_{ij}^l[\mathbf{n}, \mathbf{e}(\mathbf{x}), \mathbf{e}(\mathbf{y})] &= C_{j\alpha k \beta} e_\alpha(\mathbf{x}) n_\beta C_{i\gamma p \delta} e_\gamma(\mathbf{y}) n_\delta P_{pk}^l(\mathbf{n}). \end{aligned} \quad (13)$$

In Eq. (11), \hat{h}_{ij} is defined by

$$\hat{h}_{ij}(\mathbf{x}, \mathbf{y}; t) = C_{j\alpha k \beta} e_\alpha(\mathbf{x}) \frac{\partial g_{ik}(\mathbf{x}, \mathbf{y}; t)}{\partial x_\beta}. \quad (14)$$

It should be noted here that the time-domain displacement BIEs (3) contain strongly singular integrals, while the time-domain traction BIEs (11) have a hypersingularity at $\mathbf{y} = \mathbf{x}$.

3 Time-domain fundamental solutions for anisotropic linear elastic solids

Wang and Achenbach (1994) showed that the time-domain displacement fundamental solution for anisotropic solids can be decomposed into singular static and regular dynamic terms as

$$\begin{aligned} g_{ik}(\mathbf{x}, \mathbf{y}; t) * f_i(\mathbf{y}, t) &= g_{ik}^S(\mathbf{x}, \mathbf{y}) f_i(\mathbf{y}, t) + g_{ik}^R(\mathbf{x}, \mathbf{y}; t) * \dot{f}_i(\mathbf{y}, t). \end{aligned} \quad (15)$$

The singular static part has the following closed-form expression

$$\begin{aligned} g_{ik}^S(\mathbf{x}, \mathbf{y}) &= \frac{1}{\pi} \text{Im} \sum_{l=1}^L \frac{A_{ik}(\eta_l)}{\partial_\eta D(\eta_l)} \log[\mathbf{d}_l(\mathbf{y} - \mathbf{x})] + D_{ik}, \\ &(L = 3), \end{aligned} \quad (16)$$

with $\mathbf{d}_l = (1, \eta_l)$, while the regular dynamic part can be expressed only as a line-integral over a unit-circle

$$g_{ik}^R(\mathbf{x}, \mathbf{y}; t) = \frac{H(t)}{4\pi^2} \int_{|n|=1} \sum_{l=1}^L \frac{P_{ik}^l}{\rho c_l^2} \log |c_l t + \mathbf{n} \cdot (\mathbf{y} - \mathbf{x})| d\mathbf{n}. \quad (17)$$

The constant term D_{ik} in the static displacement fundamental solution (16) is defined by

$$D_{ik} = -\frac{1}{4\pi^2} \int_{|n|=1} \Gamma_{ik}^{-1}(n_1, n_2) \log |n_1| d\mathbf{n} \\ = -\frac{1}{\pi} \sum_{l=1}^L \frac{A_{ik}(\eta_l)}{\partial_\eta D(\eta_l)} \log(\eta_l + i). \quad (18)$$

It should be mentioned here that this term is inessential in elastostatic BIE formulations. However, to maintain the quiescent field ahead of the wave fronts caused by a point force the constant term (18) is required for elastodynamic problems. The functions $A_{ik}(\eta)$ and $D(\eta)$ in Eq. (16) can be expressed as

$$A_{ik}(\eta) = \text{adj}[\Gamma_{ik}(1, \eta)], \quad D(\eta) = \det[\Gamma_{ik}(1, \eta)], \quad (19)$$

where

$$\Gamma_{ik}(1, \eta) = L_{ik}\eta^2 + (M_{ik} + M_{ik}^T)\eta + N_{ik}, \quad (20) \\ L_{ik} = C_{2ik2}, \quad M_{ik} = C_{2ik1}, \quad N_{ik} = C_{1ik1}.$$

Moreover, the complex variable η_l in Eq. (16) denotes the distinct roots of the following sixth-order characteristic polynomial

$$D(\eta_l) = 0 \quad \text{with } \text{Im}(\eta_l) > 0. \quad (21)$$

Equation (21) has three distinct roots η_l ($l = 1, 2, 3$) for generally anisotropic solids.

The derivative $\partial_\eta D(\eta_l)$ can be written as

$$\partial_\eta D(\eta_l) = [D(\eta_l)/(\eta - \eta_l)] \quad \text{at } \eta = \eta_l. \quad (22)$$

In accordance with the decomposition of the displacement fundamental solution, the higher-order

elastodynamic fundamental solutions (6), (12) and (14) can be also separated into singular static and regular dynamic terms as

$$h_{ik}(\mathbf{x}, \mathbf{y}; t) * u_i(\mathbf{y}, t) = h_{ik}^S(\mathbf{x}, \mathbf{y}) u_i(\mathbf{y}, t) + h_{ik}^R(\mathbf{x}, \mathbf{y}; t) * \ddot{u}_i(\mathbf{y}, t), \quad (23)$$

$$\hat{h}_{ij}(\mathbf{x}, \mathbf{y}; t) * f_i(\mathbf{y}, t) = \hat{h}_{ij}^S(\mathbf{x}, \mathbf{y}) f_i(\mathbf{y}, t) + \hat{h}_{ij}^R(\mathbf{x}, \mathbf{y}; t) * \ddot{f}_i(\mathbf{y}, t), \quad (24)$$

$$w_{ij}(\mathbf{x}, \mathbf{y}; t) * u_i(\mathbf{y}, t) = w_{ij}^S(\mathbf{x}, \mathbf{y}) u_i(\mathbf{y}, t) + w_{ij}^R(\mathbf{x}, \mathbf{y}; t) * \ddot{u}_i(\mathbf{y}, t). \quad (25)$$

Substitution of Eq. (16) into Eqs. (6), (12) and (14) and application of the Stroh's formalism yield the following closed-form expressions for the static parts of the higher-order fundamental solutions

$$h_{ik}^S(\mathbf{x}, \mathbf{y}) = \frac{1}{\pi} \frac{\partial}{\partial s_y} \text{Im} \sum_{l=1}^L \frac{B_{ik}(\eta_l)}{\partial_\eta D(\eta_l)} \log[\mathbf{d}_l(\mathbf{y} - \mathbf{x})], \quad (26)$$

$$\hat{h}_{ij}^S(\mathbf{x}, \mathbf{y}) = \frac{1}{\pi} \frac{\partial}{\partial s_x} \text{Im} \sum_{l=1}^L \frac{B_{ij}(\eta_l)}{\partial_\eta D(\eta_l)} \log[\mathbf{d}_l(\mathbf{y} - \mathbf{x})], \quad (27)$$

$$w_{ij}^S(\mathbf{x}, \mathbf{y}) = \frac{1}{\pi} \frac{\partial}{\partial s_x} \frac{\partial}{\partial s_y} \text{Im} \sum_{l=1}^L \frac{C_{ij}(\eta_l)}{\partial_\eta D(\eta_l)} \log[\mathbf{d}_l(\mathbf{y} - \mathbf{x})], \quad (28)$$

where

$$B_{ik}(\eta) = (L_{ip}\eta + M_{ip}) A_{pk}, \quad (29) \\ C_{ij}(\eta) = (L_{ip}\eta + M_{ip}) A_{pk} (L_{jk}\eta + M_{jk}).$$

In Eqs. (26)-(28), the vectors \mathbf{s}_x and \mathbf{s}_y represent the unit tangent vectors on the crack-face and the external boundary at \mathbf{x} and \mathbf{y} (see Fig. 1). Moreover, $\partial/\partial s_x$ and $\partial/\partial s_y$ denote the tangential derivatives with respect to s_x and s_y . In the case of

$\mathbf{y} = \mathbf{x}$, Eqs. (26) and (27) involve a strong singularity, while Eq. (28) contains a hypersingularity

The regular dynamic parts of the higher-order fundamental solutions can be expressed as

$$h_{ik}^R(\mathbf{x}, \mathbf{y}; t) = \frac{H(t)}{4\pi^2} \int_{|\mathbf{n}|=1} \sum_{l=1}^L \frac{Q_{ik}^l[\mathbf{n}, \mathbf{e}(\mathbf{y})]}{\rho c_l^3} \times \log |c_l t + \mathbf{n} \cdot (\mathbf{y} - \mathbf{x})| d\mathbf{n}, \quad (30)$$

$$\hat{h}_{ij}^R(\mathbf{x}, \mathbf{y}; t) = -\frac{H(t)}{4\pi^2} \int_{|\mathbf{n}|=1} \sum_{l=1}^L \frac{Q_{ij}^l[\mathbf{n}, \mathbf{e}(\mathbf{x})]}{\rho c_l^3} \times \log |c_l t + \mathbf{n} \cdot (\mathbf{y} - \mathbf{x})| d\mathbf{n}, \quad (31)$$

$$w_{ij}^R(\mathbf{x}, \mathbf{y}; t) = -\frac{H(t)}{4\pi^2} \int_{|\mathbf{n}|=1} \sum_{l=1}^L \frac{R_{ij}^l[\mathbf{n}, \mathbf{e}(\mathbf{x}), \mathbf{e}(\mathbf{y})]}{\rho c_l^3} \times \frac{1}{c_l t + \mathbf{n} \cdot (\mathbf{y} - \mathbf{x})} d\mathbf{n}. \quad (32)$$

4 Numerical solution procedure

A collocation method is developed to solve the strongly singular and hypersingular time-domain BIEs. The external boundary and the crack-face are discretized into E straight elements Γ_e

$$\Gamma = \Gamma_{ex} + \Gamma_c = \sum_{e=1}^E \Gamma_e, \quad (33)$$

while the time t is divided into M constant time-steps Δt , i.e. $t = M\Delta t$. The total element-number is given by $E = E_{ex} + E_c$, where E_{ex} is the element-number for the external boundary and E_c is the element-number for the crack-face, respectively.

The unknown CODs, the displacements over the external boundary, and the tractions over the crack-face as well as the external boundary are approximated by the following interpolation functions

$$\Delta u_i(\mathbf{y}, \tau) = \sum_{e=1}^{E_c} \sum_{m=1}^M \mu_{e(\Delta u)}(\mathbf{y}) \cdot \eta_{(\Delta u)}^m(\tau) \cdot (\Delta u_i)_e^m, \quad (34)$$

$$u_i(\mathbf{y}, \tau) = \sum_{e=1}^{E_{ex}} \sum_{m=1}^M \mu_{e(u)}(\mathbf{y}) \cdot \eta_{(u)}^m(\tau) \cdot (u_i)_e^m, \quad (35)$$

$$f_i(\mathbf{y}, \tau) = \sum_{e=1}^{E_{ex}+E_c} \sum_{m=1}^M \mu_{e(f)}(\mathbf{y}) \cdot \eta_{(f)}^m(\tau) \cdot (f_i)_e^m. \quad (36)$$

A linear temporal shape-function $\eta_{(\cdot)}^m(\tau)$ is used for the temporal approximation of the boundary data

$$\eta_{(\cdot)}^m(\tau) = \frac{1}{\Delta t} \{ [\tau - (m-1)\Delta t] H[\tau - (m-1)\Delta t] - 2[\tau - m\Delta t] H[\tau - m\Delta t] + [\tau - (m+1)\Delta t] H[\tau - (m+1)\Delta t] \}. \quad (37)$$

Two different spatial shape-functions $\mu_{e(\cdot)}(\mathbf{y})$ are implemented for the spatial approximation of the boundary data. On the external boundary and on the crack-face away from the crack-tips, a piecewise constant spatial shape-function is applied

$$\mu_{e(u)}(\mathbf{y}) = \mu_{e(\Delta u)}(\mathbf{y}) = \mu_{e(f)}(\mathbf{y}) = \begin{cases} 1, & \mathbf{y} \in \Gamma_e, \\ 0, & \mathbf{y} \notin \Gamma_e, \end{cases} \quad (38)$$

while on the crack-face near the crack-tips a “square-root” crack-tip shape-function is adopted. The use of special crack-tip shape-function ensures a proper description of the local behavior of the CODs at the crack-tips and thus an accurate computation of the dynamic SIFs.

After substituting the interpolation functions (34)-(36) into the BIEs (3) and (11) and after collocating them at the E discrete points, a system of linear algebraic equations for the unknown boundary

data is obtained as

$$\begin{aligned} & \delta_d(u_k)_d^M \\ &= \sum_{e=1}^{E_{ex}} G_{ik(f)}^S(d, e)(f_i)_e^M - \sum_{e=1}^{E_{ex}} H_{ik(u)}^S(d, e)(u_i)_e^M \\ &+ \sum_{e=1}^{E_c} H_{ik(\Delta u)}^S(d, e)(\Delta u_i)_e^M \\ &+ \sum_{m=1}^M \sum_{e=1}^{E_{ex}} G_{ik(f)}^R(d, e; M-m+1)(f_i)_e^m \\ &+ \sum_{e=1}^{E_c} H_{ik(\Delta u)}^R(d, e)(\Delta u_i)_e^M \\ &+ \sum_{m=1}^M \sum_{e=1}^{E_c} H_{ik(\Delta u)}^R(d, e; M-m+1)(\Delta u_i)_e^m, \\ & \mathbf{x}_d \in \Gamma_{ex}, \end{aligned} \tag{39}$$

$$\begin{aligned} & \delta_d(f_j)_d^M \\ &= \sum_{e=1}^{E_{ex}} H_{ij(f)}^S(d, e)(f_i)_e^M - \sum_{e=1}^{E_{ex}} W_{ij(u)}^S(d, e)(u_i)_e^M \\ &+ \sum_{e=1}^{E_c} W_{ij(\Delta u)}^S(d, e)(\Delta u_i)_e^M \\ &+ \sum_{m=1}^M \sum_{e=1}^{E_{ex}} H_{ij(f)}^R(d, e; M-m+1)(f_i)_e^m \\ &- \sum_{m=1}^M \sum_{e=1}^{E_{ex}} W_{ij(u)}^R(d, e; M-m+1)(u_i)_e^m \\ &+ \sum_{m=1}^M \sum_{e=1}^{E_c} W_{ij(\Delta u)}^R(d, e; M-m+1)(\Delta u_i)_e^m, \\ & \mathbf{x}_d \in \Gamma_c. \end{aligned} \tag{40}$$

In Eqs. (39) and (40)

$$\delta_d = \begin{cases} 1/2, \mathbf{x}_d \in \Gamma_{ex}, \\ 0, \mathbf{x}_d \in \Gamma_c, \end{cases} \tag{41}$$

$$\begin{aligned} & G_{ik(f)}^S(d, e) = \\ & \int_{\Gamma_e} \left\{ \frac{1}{\pi} \text{Im} \sum_{l=1}^L \frac{A_{ik}(\eta_l)}{\partial_{\eta} D(\eta_l)} \log[\mathbf{d}_l(\mathbf{y} - \mathbf{x}_d)] + D_{ik} \right\} \times \\ & \mu_{e(f)}(\mathbf{y}) ds_y, \end{aligned} \tag{42}$$

$$\begin{aligned} & H_{ik(u)}^S(d, e) = \\ & \int_{\Gamma_e} \frac{1}{\pi} \frac{\partial}{\partial s_y} \text{Im} \sum_{l=1}^L \frac{B_{ik}(\eta_l)}{\partial_{\eta} D(\eta_l)} \log[\mathbf{d}_l(\mathbf{y} - \mathbf{x}_d)] \times \\ & \mu_{e(u)}(\mathbf{y}) ds_y, \end{aligned} \tag{43}$$

$$\begin{aligned} & H_{ik(\Delta u)}^S(d, e) = \\ & \int_{\Gamma_e} \frac{1}{\pi} \frac{\partial}{\partial s_y} \text{Im} \sum_{l=1}^L \frac{B_{ik}(\eta_l)}{\partial_{\eta} D(\eta_l)} \log[\mathbf{d}_l(\mathbf{y} - \mathbf{x}_d)] \times \\ & \mu_{e(\Delta u)}(\mathbf{y}) ds_y, \end{aligned} \tag{44}$$

$$\begin{aligned} & H_{ij(f)}^S(d, e) = \\ & \int_{\Gamma_e} \frac{1}{\pi} \frac{\partial}{\partial s_x} \text{Im} \sum_{l=1}^L \frac{B_{ij}(\eta_l)}{\partial_{\eta} D(\eta_l)} \log[\mathbf{d}_l(\mathbf{y} - \mathbf{x}_d)] \times \\ & \mu_{e(f)}(\mathbf{y}) ds_y, \end{aligned} \tag{45}$$

$$\begin{aligned} & W_{ij(u)}^S(d, e) = \\ & \int_{\Gamma_e} \frac{1}{\pi} \frac{\partial}{\partial s_x} \frac{\partial}{\partial s_y} \text{Im} \sum_{l=1}^L \frac{C_{ij}(\eta_l)}{\partial_{\eta} D(\eta_l)} \log[\mathbf{d}_l(\mathbf{y} - \mathbf{x}_d)] \times \\ & \mu_{e(u)}(\mathbf{y}) ds_y, \end{aligned} \tag{46}$$

$$\begin{aligned} & W_{ij(\Delta u)}^S(d, e) = \\ & \int_{\Gamma_e} \frac{1}{\pi} \frac{\partial}{\partial s_x} \frac{\partial}{\partial s_y} \text{Im} \sum_{l=1}^L \frac{C_{ij}(\eta_l)}{\partial_{\eta} D(\eta_l)} \log[\mathbf{d}_l(\mathbf{y} - \mathbf{x}_d)] \times \\ & \mu_{e(\Delta u)}(\mathbf{y}) ds_y, \end{aligned} \tag{47}$$

$$\begin{aligned} & G_{ik(f)}^R(d, e; M-m+1) = \\ & \int_{(m-1)\Delta t}^{(m+1)\Delta t} \frac{H(t)}{4\pi^2} I_{ik}(d, e; \tau) \dot{\eta}_{(f)}^m(\tau) d\tau, \end{aligned} \tag{48}$$

$$\begin{aligned} & H_{ik(u)}^R(d, e; M-m+1) = \\ & \int_{(m-1)\Delta t}^{(m+1)\Delta t} \frac{H(t)}{4\pi^2} J_{ik}(d, e; \tau) \ddot{\eta}_{(u)}^m(\tau) d\tau, \end{aligned} \tag{49}$$

$$H_{ik(\Delta u)}^R(d, e; M - m + 1) = \int_{(m-1)\Delta t}^{(m+1)\Delta t} \frac{H(t)}{4\pi^2} K_{ik}(d, e; \tau) \ddot{\eta}_{(\Delta u)}^m(\tau) d\tau, \quad (50)$$

$$H_{ij(f)}^R(d, e; M - m + 1) = \int_{(m-1)\Delta t}^{(m+1)\Delta t} \frac{H(t)}{4\pi^2} S_{ij}(d, e; \tau) \ddot{\eta}_{(f)}^m(\tau) d\tau, \quad (51)$$

$$W_{ij(u)}^R(d, e; M - m + 1) = \int_{(m-1)\Delta t}^{(m+1)\Delta t} \frac{H(t)}{4\pi^2} T_{ij}(d, e; \tau) \ddot{\eta}_{(u)}^m(\tau) d\tau, \quad (52)$$

$$W_{ij(\Delta u)}^R(d, e; M - m + 1) = \int_{(m-1)\Delta t}^{(m+1)\Delta t} \frac{H(t)}{4\pi^2} U_{ij}(d, e; \tau) \ddot{\eta}_{(\Delta u)}^m(\tau) d\tau, \quad (53)$$

where

$$t = t_M - \tau, \quad (54)$$

$$I_{ik}(d, e, t) = \int_{\Gamma_e} \int_{|n|=1} \sum_{l=1}^L \frac{P_{ik}^l}{\rho c_l^2} \log |c_l t + \mathbf{n} \cdot (\mathbf{y} - \mathbf{x}_d)| \times d\mathbf{n} \mu_{e(f)}(\mathbf{y}) ds_y, \quad (55)$$

$$J_{ik}(d, e, t) = \int_{\Gamma_e} \int_{|n|=1} \sum_{l=1}^L \frac{Q_{ik}^l[\mathbf{n}, \mathbf{e}(\mathbf{y})]}{\rho c_l^3} \times \log |c_l t + \mathbf{n} \cdot (\mathbf{y} - \mathbf{x}_d)| d\mathbf{n} \mu_{e(u)}(\mathbf{y}) ds_y, \quad (56)$$

$$K_{ik}(d, e, t) = \int_{\Gamma_e} \int_{|n|=1} \sum_{l=1}^L \frac{Q_{ik}^l[\mathbf{n}, \mathbf{e}(\mathbf{y})]}{\rho c_l^3} \times \log |c_l t + \mathbf{n} \cdot (\mathbf{y} - \mathbf{x}_d)| d\mathbf{n} \mu_{e(\Delta u)}(\mathbf{y}) ds_y, \quad (57)$$

$$S_{ij}(d, e, t) = - \int_{\Gamma_e} \int_{|n|=1} \sum_{l=1}^L \frac{Q_{ij}^l[\mathbf{n}, \mathbf{e}(\mathbf{x})]}{\rho c_l^3} \times \log |c_l t + \mathbf{n} \cdot (\mathbf{y} - \mathbf{x}_d)| d\mathbf{n} \mu_{e(f)}(\mathbf{y}) ds_y, \quad (58)$$

$$T_{ij}(d, e, t) = - \int_{\Gamma_e} \int_{|n|=1} \sum_{l=1}^L \frac{R_{ij}^l}{\rho c_l^3} \frac{1}{c_l t + \mathbf{n} \cdot (\mathbf{y} - \mathbf{x}_d)} \times d\mathbf{n} \mu_{e(u)}(\mathbf{y}) ds_y, \quad (59)$$

$$U_{ij}(d, e, t) = - \int_{\Gamma_e} \int_{|n|=1} \sum_{l=1}^L \frac{R_{ij}^l}{\rho c_l^3} \frac{1}{c_l t + \mathbf{n} \cdot (\mathbf{y} - \mathbf{x}_d)} \times d\mathbf{n} \mu_{e(\Delta u)}(\mathbf{y}) ds_y. \quad (60)$$

To compute the system matrices containing strongly singular and hypersingular boundary integrals, special analytical and numerical techniques are developed. Time integrations arising in the system matrices are carried out analytically. In the case of constant shape-functions spatial integrations can also be performed analytically, while in the case of crack-tip shape-functions analytical and numerical integrations are required. The line-integrals over a unit-circle in the dynamic part of the fundamental solutions are computed numerically. Finally, the present time-domain BEM yields an explicit time-stepping scheme for computing the time-dependent CODs and other unknown boundary quantities.

5 Computation of dynamic stress intensity factors

After the time-dependent CODs have been computed numerically by using the time-domain BEM as presented in the previous section, the mode-I and the mode-II elastodynamic SIFs can be obtained directly from the CODs. For this purpose, the following relation between the elastodynamic SIFs and the CODs is applied (Sih, Paris and Irwin, 1965; Zhang, 2004)

$$\begin{Bmatrix} K_I(t) \\ K_{II}(t) \end{Bmatrix} = \frac{\sqrt{2\pi}}{4\Delta} \begin{bmatrix} H_{11} & H_{12} \\ H_{21} & H_{22} \end{bmatrix} \lim_{r \rightarrow 0} \frac{1}{\sqrt{r}} \begin{Bmatrix} \Delta u_1(r, t) \\ \Delta u_2(r, t) \end{Bmatrix}, \quad (61)$$

where

$$\begin{bmatrix} H_{11} & H_{12} \\ H_{21} & H_{22} \end{bmatrix} = \begin{bmatrix} \text{Im} \left(\frac{q_1 - q_2}{\mu_1 - \mu_2} \right) & \text{Im} \left(\frac{p_2 - p_1}{\mu_1 - \mu_2} \right) \\ \text{Im} \left(\frac{\mu_1 q_2 - \mu_2 q_1}{\mu_1 - \mu_2} \right) & \text{Im} \left(\frac{\mu_2 p_1 - \mu_1 p_2}{\mu_1 - \mu_2} \right) \end{bmatrix}, \quad (62)$$

and

$$\Delta = H_{11}H_{22} - H_{12}H_{21}. \quad (63)$$

In Eq. (61), r denotes the distance from the crack-tip to the collocation point closest to the crack-tip, and μ_α are the two complex roots of the following characteristic equation

$$b_{11}\mu_\alpha^4 - 2b_{16}\mu_\alpha^3 + (2b_{12} + b_{66})\mu_\alpha^2 - 2b_{26}\mu_\alpha + b_{22} = 0, \quad (64)$$

where b_{ij} ($i, j = 1, 2, 6$) represents the compliance matrix of the anisotropic solids, and

$$\begin{aligned} p_\alpha &= b_{11}\mu_\alpha^2 + b_{12} - b_{16}\mu_\alpha, \\ q_\alpha &= (b_{12}\mu_\alpha^2 + b_{22} - b_{26}\mu_\alpha) / \mu_\alpha. \end{aligned} \quad (65)$$

6 Numerical examples

To illustrate the accuracy and the efficiency of the present time-domain BEM, numerical examples are presented in this section.

6.1 A finite crack in an infinite anisotropic solid

In the first numerical example, we consider a finite crack of length $2a$ in an infinite, anisotropic and linear elastic solid subjected to an impact tensile loading as shown in Fig. 2.

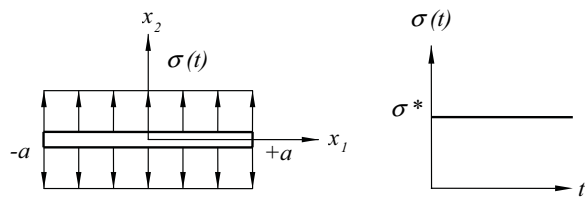


Figure 2: A finite crack in an infinite anisotropic solid subjected to an impact tensile loading

Numerical calculations are carried out for the following elastic constants, which correspond to Graphite-epoxy composite with a composition of

65% graphite and 35% epoxy

$$C_{ij} = \begin{bmatrix} 95.46 & 28.93 & 4.03 & 0 & 0 & 44.67 \\ & 25.91 & 4.65 & 0 & 0 & 15.56 \\ & & 16.34 & 0 & 0 & 0.54 \\ & & & 4.4 & -1.78 & 0 \\ & sym & & & 6.45 & 0 \\ & & & & & 32.68 \end{bmatrix} \text{GPa},$$

$$\rho = 1600 \text{kg/m}^3.$$

For convenience, the mode-I and the mode-II dynamic SIFs are normalized by

$$\bar{K}_i(t) = K_i(t) / K_I^{st}, \quad (i = I, II), \quad (66)$$

with

$$K_I^{st} = \sigma \sqrt{\pi a}, \quad (67)$$

where σ is the amplitude of the impact tensile loading, and a is the half crack-length.

For the discretization of the crack-face a total number of 20 elements is chosen and a time-step $c_T \Delta t / a = 0.1$ is used, where $c_T = \sqrt{C_{66} / \rho}$ represents the transverse wave velocity.

In Figs. 3 and 4 the numerical results for the normalized dynamic SIFs $\bar{K}_I(t)$ and $\bar{K}_{II}(t)$ versus the dimensionless time $c_T t / a$ are presented. A comparison with the numerical results obtained by other time-domain BEM [Hirose, Zhang and Wang (2002) and Zhang, Savaidis and Savaidis (2001)] shows a very good agreement.

Then, we consider a finite crack in an infinite anisotropic solid subjected to an impact shear loading as shown in Fig. 5. The same element number and time-step as in the previous example are applied. In this case, the mode-I and the mode-II dynamic SIFs are normalized by

$$\bar{K}_i(t) = K_i(t) / K_{II}^{st}, \quad (i = I, II), \quad (68)$$

where

$$K_{II}^{st} = \tau \sqrt{\pi a}, \quad (69)$$

with τ being the amplitude of the impact shear loading, and a is the half crack-length.

The corresponding normalized mode-I and mode-II dynamic SIFs versus the dimensionless time $c_T t / a$ are presented in Figs. 6 and 7. Here again, one can see a quite good agreement with the numerical results of Hirose, Zhang and Wang (2002) and Zhang, Savaidis and Savaidis (2001).

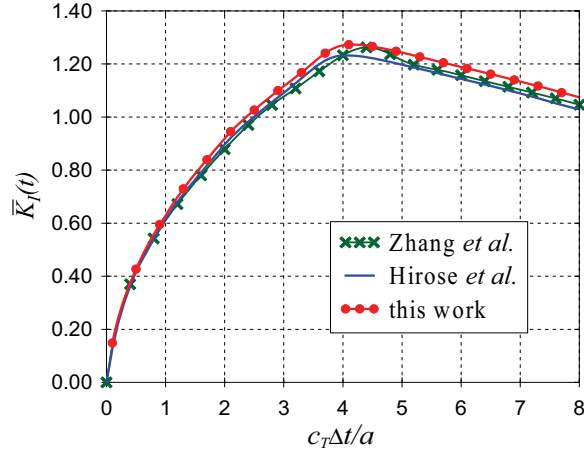


Figure 3: $\bar{K}_I(t)$ for an impact tensile crack-face loading

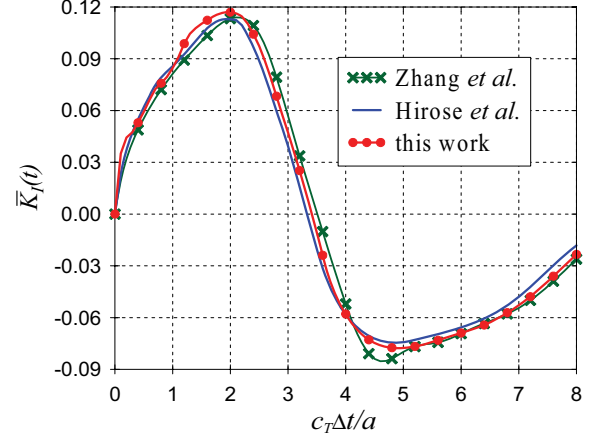


Figure 6: $\bar{K}_I(t)$ for an impact shear crack-face loading

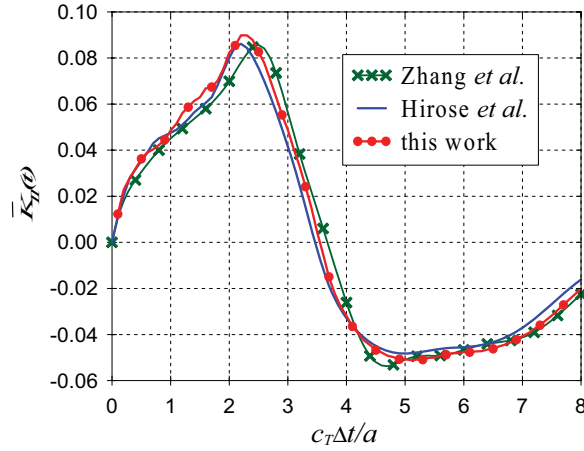


Figure 4: $\bar{K}_{II}(t)$ for an impact tensile crack-face loading

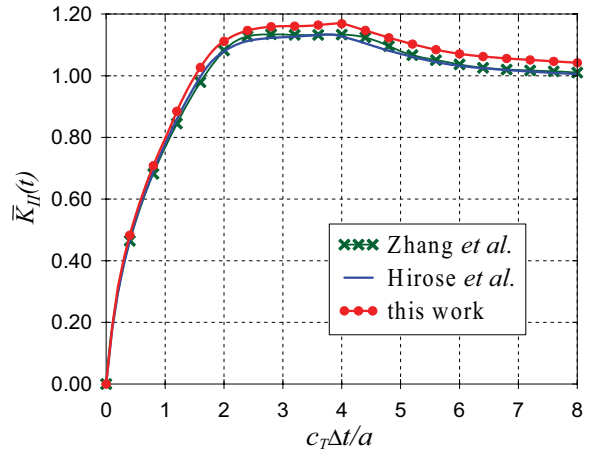


Figure 7: $\bar{K}_{II}(t)$ for an impact shear crack-face loading

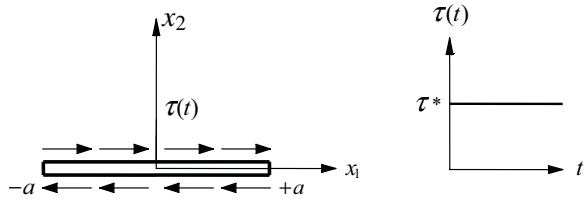


Figure 5: A finite crack in an infinite anisotropic solid subjected to an impact shear loading

6.2 A central crack in a finite anisotropic plate

In the second numerical example, we consider a central crack in a rectangular orthotropic plate subjected to an impact loading normal to the crack-face as illustrated in Fig. 8. The plate ge-

ometry is defined by $2w = 20\text{mm}$, $2h = 40\text{mm}$ and $2a = 4.8\text{mm}$. The following material constants are used in the numerical calculations: Young's moduli $E_1 = 118.3\text{GPa}$, $E_2 = 54.3\text{GPa}$, shear modulus $G_{12} = 8.79\text{GPa}$, Poisson's ratio $\nu_{12} = 0.083$ and mass density $\rho = 1900\text{kg/m}^3$. Plane stress condition is assumed.

The cracked plate is discretized into 136 elements, 42 for the horizontal boundaries, 84 for the vertical boundaries and 10 for the crack-face. The time-step is taken as $\Delta t = 2a/(10c_T) = 0,223\mu\text{s}$ with $c_T \Delta t / \Delta l_{crack} = 1.0$, where Δl_{crack} is the element-length of the crack-face.

Figure 9 shows the normalized mode-I dynamic

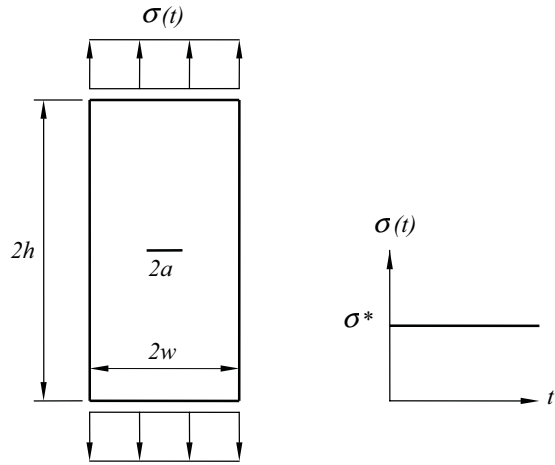


Figure 8: A central crack in a rectangular orthotropic plate

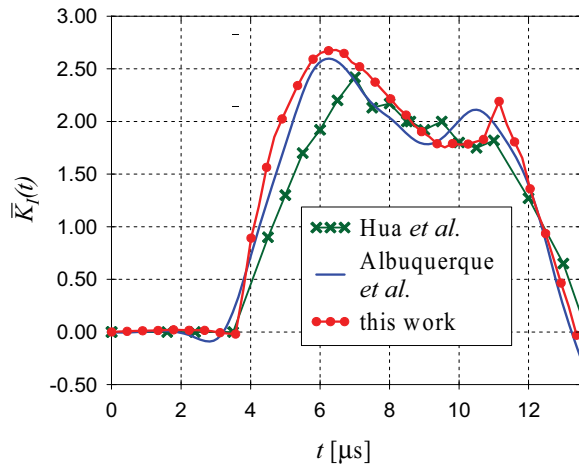


Figure 9: Normalized mode-I dynamic stress intensity factor for a rectangular orthotropic plate with a central crack

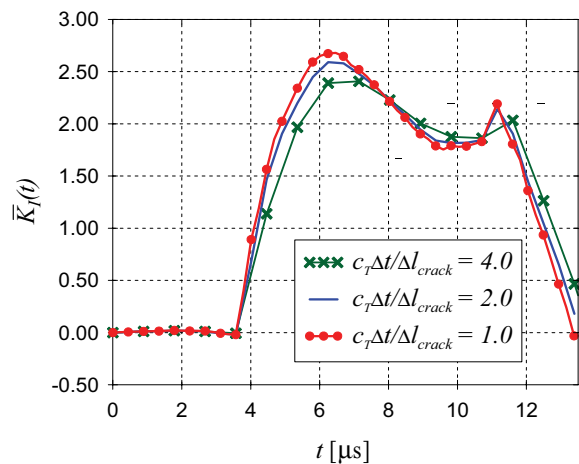


Figure 10: Effects of the time-step on the normalized mode-I dynamic stress intensity factor

SIF versus time t . A comparison of our numerical results with that of Albuquerque, Sollero and Aliabadi (2004) using a dual boundary element method and with Hua, Tian-You and Lan-Quao (1996) using a finite-difference method shows a satisfactory agreement. Although there is a small deviation in the maximum value of $\bar{K}_I(t)$ from the maximum values of Albuquerque, Sollero and Aliabadi (2004) and Hua, Tian-You and Lan-Quao (1996), the global behavior of the three different curves is very similar.

As is well known for the explicit time-stepping scheme, the accuracy and the quality of the present time-domain BEM are dependent on the selected time-step. The effect of the used time-step on the normalized mode-I dynamic stress intensity factor is presented in Fig. 10. Stable and accurate results can be achieved for a time-step $c_T \Delta t / \Delta l_{crack} = 1.0$. Smaller time-steps such as $c_T \Delta t / \Delta l_{crack} = 0.8$ lead to unstable numerical results for $\bar{K}_I(t)$. On the other hand, for larger time-steps such as $c_T \Delta t / \Delta l_{crack} = 4.0$, unrealistically large numerical damping occurs in $\bar{K}_I(t)$ and the results become less accurate.

6.3 A slanted edge crack in an orthotropic plate

In the last numerical example, a rectangular orthotropic plate with a slanted edge crack subjected to an impact tensile loading is investigated, see Fig. 11. Plane stress condition is assumed and the following geometrical parameters are considered: $w=32\text{mm}$, $h=44\text{mm}$, $c=6\text{mm}$, $a=22.63\text{mm}$ and $\alpha = 45^\circ$. The used orthotropic material properties are: Young's moduli $E_1 = 82.4\text{GPa}$, $E_2 = 164.8\text{GPa}$, shear modulus $G_{12} = 29.4\text{GPa}$, Poisson's ratio $\nu_{12} = 0.4006$ and mass density $\rho = 2450\text{kg/m}^3$. The cracked plate is discretized by a total number of 50 elements, 8 for the crack-face, 24 for the horizontal boundaries and 18 for the vertical boundaries. The time-step is selected as $\Delta t = 0.866\mu\text{s}$ corresponding to $c_T \Delta t / \Delta l_{crack} = 1.06$, where c_T represents the transverse wave velocity and Δl_{crack} is the element-length of the crack-face, respectively.

In Figs. 12 and 13, the numerical results for the normalized mode-I and mode-II dynamic

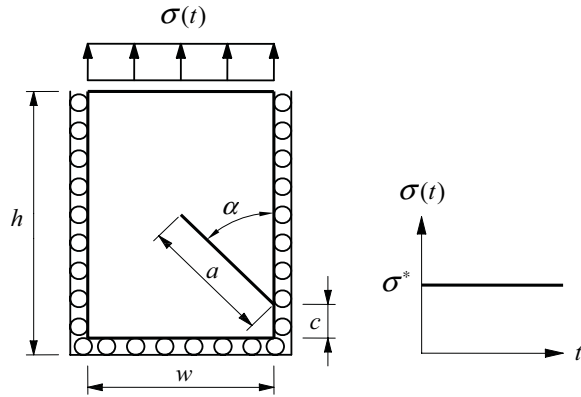


Figure 11: A slanted edge crack in a rectangular orthotropic plate

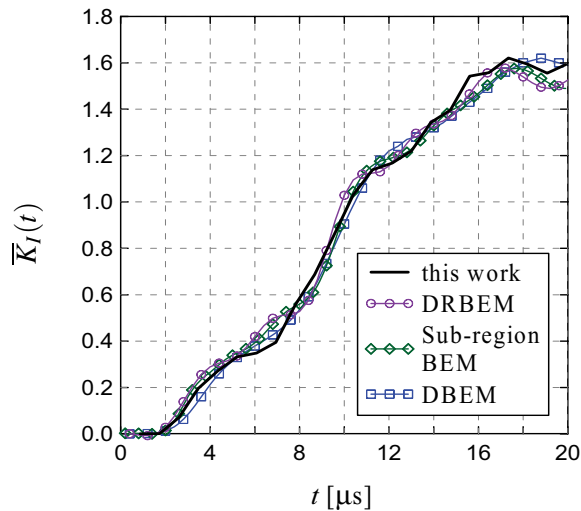


Figure 12: Normalized mode-I dynamic stress intensity factor for a slanted edge crack

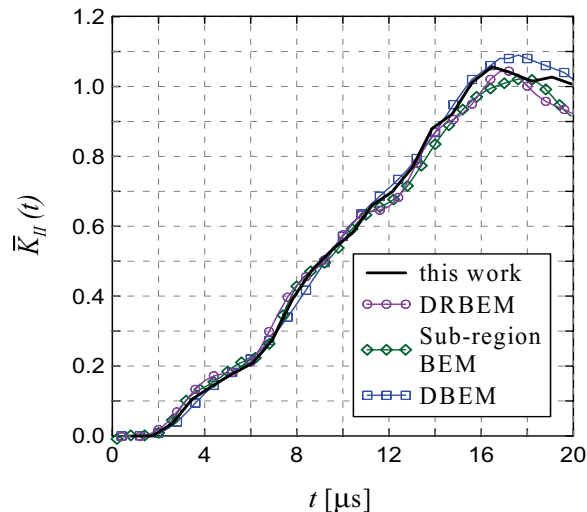


Figure 13: Normalized mode-II dynamic stress intensity factor for a slanted edge crack

SIFs obtained by the present time-domain BEM are presented and compared with that of Albuquerque, Sollero and Aliabadi (2002) using a sub-region BEM, Albuquerque, Sollero and Fedelinski (2003) using a dual reciprocity boundary element method (DRBEM) in the Laplace-transformed domain, and Albuquerque, Sollero and Aliabadi (2004) via a dual boundary element method (DBEM). It can be seen in Figs. 12 and 13 that the normalized dynamic SIF obtained by the present time-domain BEM agree quite well with other numerical results.

7 Conclusions

This paper presents a hypersingular time-domain BEM for transient dynamic crack analysis in 2-D, homogeneous, generally anisotropic and linear elastic solids. In particular, a finite crack in an infinite or a finite solid subjected to impact loading conditions is investigated. For this purpose, a time-domain boundary integral equation formulation is developed, which uses a combination of the classical displacement BIEs for the external boundary and the hypersingular traction BIEs for the crack-face. To solve the time-domain BIEs numerically, a numerical solution procedure based on a collocation method for both the temporal and spatial discretizations is developed. Time integrations are carried out analytically, while strongly singular and hypersingular spatial integrals are computed by special analytical and numerical integration techniques. Integrations over the unit-circle arising in the elastodynamic fundamental solutions are performed numerically. An explicit time-stepping scheme is finally obtained to compute the discrete CODs and other unknown boundary data. Special crack-tip shape functions are adopted at the crack-tips to properly describe the local behavior of the CODs at the crack-tips. This ensures an accurate and direct computation of the dynamic SIFs from the numerically determined CODs. To verify the accuracy and the efficiency of the present time-domain BEM for transient dynamic crack analysis in 2-D homogeneous, generally anisotropic and linear elastic solids, numerical examples for both infinite and finite domains containing a central crack or an edge

crack are presented and discussed. Comparisons of the present numerical results for the normalized dynamic stress intensity factors with that obtained by other numerical methods show a good agreement.

Acknowledgement: This work is supported by the German Research Foundation (DFG) under the project numbers ZH 15/5-1 and ZH 15/5-2, which is gratefully acknowledged.

References

- Albuquerque, E. L.; Sollero, P.; Aliabadi, M. H.** (2002): The boundary element method applied to time dependent problems in anisotropic materials. *Int. J. Solids Struct.*, vol. 32, pp. 1405-1422.
- Albuquerque, E. L.; Sollero, P.; Fedelinski, P.** (2003): Dual reciprocity boundary element method in Laplace domain applied to anisotropic dynamic crack problems. *Comput. & Struct.*, vol. 81, pp. 1703-1713.
- Albuquerque, E. L.; Sollero, P.; Aliabadi, M. H.** (2004): Dual boundary element method for anisotropic dynamic fracture mechanics. *Int. J. Numer. Meth. Eng.*, vol. 59, pp. 1187-1205.
- Aliabadi, M. H.** (2002): The Boundary Element Method. John Wiley & Sons, New York.
- Antes, H.** (1985): A boundary element procedure for transient wave propagations in two-dimensional isotropic elastic media. *Finite Elements Anal. Design*, vol. 1, pp. 313-322 (1985).
- Antes, H.** (1987): Anwendung der Randelementmethode in der Elasto- und Fluidodynamik. Teubner-Verlag, Stuttgart.
- Beskos, D. E.** (1987): Boundary element methods in dynamic analysis. *Appl. Mech. Rev.*, vol. 40, pp. 1-23.
- Beskos, D. E.** (1997): Boundary element methods in dynamic analysis: part II (1986-1996). *Appl. Mech. Rev.*, vol. 50, pp. 149-197.
- Bonnet, H.** (1999): Boundary Integral Equation Methods for Solids and Fluids. John Wiley & Sons, New York.
- Cole, D. M.; Kosloff, D. D.; Minster, J. B.** (1978): A numerical boundary integral equation method for elastodynamics I. *Bul. Seis. Soc. Amer.*, vol. 68, pp. 1331-1357.
- Cruse, T. A.; Rizzo, F. J.** (1968): A direct formulation and numerical solution of the general transient elastodynamic problem. I. *J. Math. Anal. Appl.*, vol. 22, pp. 244-259.
- Cruse, T. A.** (1968): A direct formulation and numerical solution of the general transient elastodynamic problem. II. *J. Math. Anal. Appl.*, vol. 22, pp. 341-355.
- Dominguez, J.** (1993): Boundary Element Methods in Dynamics. Computational Mechanics Publications, Southampton, UK.
- Estorff, O. V.** (1986): Zur Berechnung der dynamischen Wechselwirkung zwischen Bauwerken und ihrer Umgebung mittels zeitabhängiger Randintegralgleichungen. Report TWM 86-10, Inst. Konstr. Ingenieurbau, Ruhr-University Bochum, Germany.
- Hirose, S.** (1999): Dynamic analysis for a crack in anisotropic elastic solid (in Japanese). *JAS-COME*, vol. 16, pp. 13-17.
- Hirose, S.; Wang, C. -Y.; Achenbach, J. D.** (2000): Boundary element method for elastic wave scattering by a crack in an anisotropic elastic solid. In: *20th International Congress for Theoretical and Applied Mechanics, ICTAM 2000*, Chicago, USA, 27 August-2 September 2000.
- Hirose, S.; Zhang, Ch.; Wang, C. -Y.** (2002): A comparative study of two time-domain BEM/BIEM for transient dynamic crack analysis of anisotropic solid. In: *Boundary Element Techniques* (Ed. by Yao, Zhenhan and Aliabadi, M.H.), Tsinghua University Press & Springer, pp. 106-112.
- Hua, Z.; Tian-You, F.; Lan-Quao, T.** (1996): Composite materials dynamic fracture studies by generalized Shmueli difference algorithm. *Eng. Fract. Mech.*, vol.54, pp. 869-877.
- Manolis, G.** (1983): A comparative study on three boundary element method approaches to problems in elastodynamics. *Int. J. Numer. Meth. Eng.*, vol. 19, pp. 73-91.
- Mansur, W. J.** (1983): A Time-Stepping Technique to Solve Wave Propagation Problems Us-

ing the Boundary Element Method. Ph.D. Thesis, University of Southampton, UK.

Niwa, Y.; Fukui, T.; Kato, S., Fuji, K. (1980): An application of the integral equation method for two-dimensional elastodynamics. *Theor. Appl. Mech.*, vol. 28, pp. 281-290.

Sih, G. C.; Paris, P. C.; Irwin, G. R. (1965): On cracks in rectilinearly anisotropic bodies. *Int. J. Fract.*, vol. 1, pp. 189-203.

Tan, A.; Hirose, S.; Zhang, Ch; Wang, C. - Y. (2005): A 2D time-domain BEM for transient wave scattering analysis by a crack in anisotropic solids. *Eng. Anal. Bound. Elem.*, vol. 29, pp. 610-623.

Tan, A.; Hirose, S.; Zhang, Ch. (2005): A time-domain collocation-Galerkin BEM for transient dynamic crack analysis in anisotropic solids. *Eng. Anal. Bound. Elem.*, vol. 29, pp. 1025-1038.

Wang, C. -Y.; Achenbach, J. D., Hirose, S. (1996): Two-dimensional time-domain BEM for scattering of elastic waves in solids of general anisotropy. *Int. J. Solids Struct.*, vol. 33, pp. 3843-3864.

Wang, C. -Y.; Achenbach, J. D. (1994): Elastodynamic fundamental solutions for anisotropic solids. *Geophys. J. Int.*, vol. 118, pp. 384-392.

Zhang, Ch. (2000): Transient elastodynamic antiplane crack analysis in anisotropic solids. *Int. J. Solids Struct.*, vol. 37, pp. 6107-6130.

Zhang, Ch.; Savaidis, A; Savaidis, G. (2001): Dynamic crack analysis of anisotropic solids under impact loading. In: *Transactions 16th Int. Conf. on Structural Mechanics in Reactor Technology* (Ed. by C. Matzen and C. C. David Tung), Center for Nuclear Power Plant Structures, Equipment and Piping, North Carolina State University, USA, Paper # 1981.

Zhang, Ch. (2002a): A 2D hypersingular time-domain BEM for transient elastodynamic crack analysis. *Wave Motion*, vol. 35, pp. 17-40.

Zhang, Ch. (2002b): A 2-D time-domain BIEM for dynamic analysis of cracked orthotropic solids. *CMES: Computer Modeling in Engineering & Sciences*, vol. 3, pp. 381-398.

Zhang, Ch. (2004): Transient dynamic crack

analysis in anisotropic solids. In: *Crack Dynamics*, Chapter 3 (Ed. by A. Ivankovic and M. H. Aliabadi), pp. 71-120, WIT Press, Southampton, Boston.

